Article

JOURNAL OF THE CHINESE CHEMICAL SOCIETY

Mechanical Properties and *In Vitro* Physico-chemical Reactivity of Gel-derived SiO_2–Na_2O–CaO–P_2O_5 Glass from Sand

Enobong R. Essien,[a]* Luqman A. Adams[b] and Femi O. Igbari[b]
[a]*Department of Chemical Sciences, Bells University of Technology, P.M.B 1015 Ota, Ogun, Nigeria*
[b]*Department of Chemistry, University of Lagos, Nigeria*

(Received: Dec. 4, 2015; Accepted: May 11, 2016; Published Online: ???; DOI: 10.1002/jccs.201500496)

In the present report, a bioactive glass was synthesized from silica sand as economic substitute to alkoxy silane reagents. Sodium metasilicate (Na_2SiO_3) obtained from the sand was hydrolyzed and gelled using appropriate reagents before sintering at 950 °C for 3 h to produce glass in the system SiO_2–Na_2O–CaO–P_2O_5. Compression test was conducted to investigate the mechanical strength of the glass, while immersion studies in simulated body fluid (SBF) was used to evaluate reactivity, bioactivity and degradability. Furthermore, the glass samples were characterized by scanning electron microscopy (SEM), X–ray diffraction (XRD), Fourier transform infrared spectroscopy (FTIR) and energy dispersive X–ray spectroscopy (EDX) to evaluate the microstructure and confirm apatite formation on the glass surface. The glass, dominated by bioactive sodium calcium silicate, $Na_2Ca_2Si_3O_9$ (combeite) crystals, had mechanical strength of 0.37 MPa and showed potentials for application as scaffold in bone repair.

Keywords: Sand; Silica source; $Na_2Ca_2Si_3O_9$; Mechanical strength; Bioactivity; Characterization.

INTRODUCTION

Skeletal regeneration has continued to gain prominence in biomedical research due to increasing clinical demand for biocompatible substitute materials for repair of damaged or diseased bones as emphasis shifts from tissue replacement to regeneration.[1,2] Certain inorganic materials capable of eliciting osteoinductive behaviour in the presence of physiological fluids are being used to act as temporary scaffolds to facilitate complete restoration of the damaged bone. Some of these materials, which include bioactive glasses and ceramics, calcium phosphates (CaP's) such as hydroxyapatite (HA), tricalcium phosphate (TCP), biphasic calcium phosphate (BCP) and biodegradable polymers in combination with inorganic materials as composites,[3,4] when used as implants, undergo a process called "bioactive fixation" forming interfacial bonds to the host tissue through the formation of biologically active hydroxyapatite (HA) layer on the surface of the implants.[5] The bond thus formed at the implant-bone interface has a strength similar to bone.

An ideal scaffold should be highly porous to allow for cell seeding and infiltration, tissue ingrowth and vascularization, as well as nutrient delivery and waste removal.[3] It is generally agreed that a minimum of 100 μm interconnected aperture pore diameter is required by the scaffold to accomplish this function *in vivo*.[6] A scaffold should also stimulate osteoblastic cell proliferation and differentiation *in vivo* while acting as a passive material during the regeneration process.[4,7]

Bioactive glasses are based on a random network of silica tetrahedra containing Si–O–Si bonds. The network can be modified by the addition of network modifiers such as Ca, Na and P, which are bonded to the network via non-bridging oxygen bonds. The mechanism of bone bonding to bioactive glasses is due to the formation of a carbonate substituted hydroxyapatite layer (HCA) on the surface of the materials after immersion in body fluid.[8,9] This layer is similar to the apatite layer in bone and, therefore, a strong bond can form.[10]

The foremost bioactive glass is the silicate-based 45S5 Bioglass® having the composition (46.1 SiO_2, 24.4 Na_2O, 26.9 CaO and 2.6 P_2O_5, in mol%),[9] which was first prepared using the melting method. This Bioglass® (Perioglas) is being used clinically to treat periodontal disease and as a bone filling material (Novabone[10,11]). Another important use of Bioglass® implants has been in the replacement of damaged middle ear bones and as tooth root replacements.[12]

The key compositional features that are responsible for the bioactivity of 45S5 glass are its low SiO_2 content (when compared to more chemically durable silicate glasses), high Na_2O and CaO content, and high CaO/P_2O_5 ratio.[13]

* Corresponding author. Tel: +2348139447446; Email: reggiessien@gmail.com

Most routes to synthesis of bioactive glasses are through the sol-gel processing method that involves the hydrolysis of alkoxide precursors to form a sol. The sol formed undergoes polycondensation to form a silica network (gel). Heat treatment of the resultant gel after aging affords the glass.[14,15] Several advantages of a sol-gel-derived glass over a melt-derived glass include; relatively lower processing temperatures,[16] higher purity and homogeneity,[16] wider compositional range of up to 100% of SiO_2 while maintaining bioactivity.[17] Additionally, the glass displays higher bioactivity and resorbability in aqueous media due to its nanometre scale textural porosity which results in a higher surface area for cation exchange, and exposure of many silanol groups to the solution to act as nucleation sites for HCA layer formation for bone bonding.[18]

The bonding to living bone of HCA layer occurs upon a sequence of reactions on the material surface[19] followed by cellular reactions. The reactions on the glass surface can be summarized to include ion leaching/exchange, dissolution of the glass network and precipitation and growth of calcium deficient carbonated apatite (HCA) surface,[8,9,19] while cellular reactions include colonization, proliferation and differentiation of relevant (bone) cells.[10]

Mechanical competence is key for application of the scaffold material in load-bearing sites. The material should be able to act as temporary support and also match the bioresorption kinetics of the damaged site pending when a new bone is formed. A limitation in the application of bioactive glasses is their low fracture toughness. Densification at high temperatures is one of the strategies to optimize the mechanical properties of bioactive glasses. In addition, inclusion of Na_2O in the composition may result in improved mechanical capability because Na_2O containing bioactive glasses transform from amorphous to glass ceramic forming hard, yet biodegradable crystalline phase $Na_2Ca_2Si_3O_9$ (combeite) when sintered.[20,21] Crystallinity is thought to have an adverse effect on the reactivity of the glass in physiological fluids, thus decreasing apatite formation and protein adsorption profile.[22] To avoid complete crystallization and its inherent effects on bioactivity of glass, a sintering protocol where the glass is partially crystallized is desirable.

Large scale preparation of bioactive glasses faces a huge challenge because of high cost of alkoxysilanes such as tetramethyl orthosilicate (TMOS) and tetraethyl orthosilicate (TEOS), which serve as precursors for SiO_2 as glass network former.[22-27] As a follow-up to our previous work[23] we report herein the study of the mechanical and dissolution behaviour in SBF of porous silicate-based quaternary bioactive glass from sand as an inexpensive substitute to alkoxysilanes.

RESULTS AND DISCUSSION

Comparison of chemical bonds present in the sodium metasilicate prepared from sand (SM) and commercial sodium metasilicate, $Na_2SiO_3.9H_2O$ (CM)

The chemical bonds present in the liquid sodium metasilicate synthesized from sand (SM) and commercial sodium metasilicate, $Na_2SiO_3.9H_2O$ (CM) (Sigma-Aldrich) as evaluated by FTIR, are shown in Figure 1, while the comparison of bond types present in the two samples are presented in Table 1. The spectra of both samples are similar showing the presence Q^n [SiO_4] silicate tetrahedra connectivity, where n is the number of bridging oxygens (BO) on the tetrahedral unit.[28] The frequencies at 893, 970 and 1196 cm^{-1} in CM (Figure 1(a) are considered for Q^0, Q^1 and Q^4 species respectively; while the spectra of SM (Figure 1(b) shows the presence of only Q^0 and Q^1 at 899 and

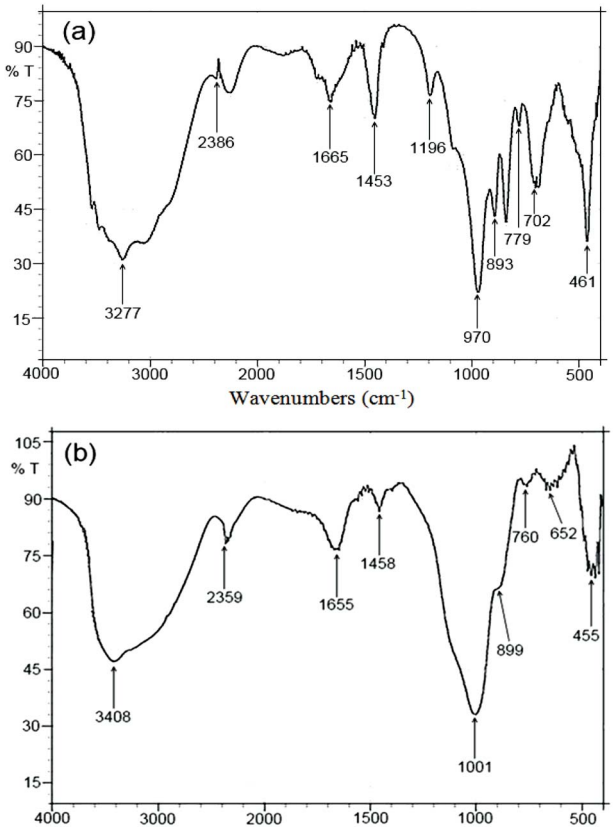

Fig. 1. FTIR spectra of CM (a) and SM (b) showing the frequencies of bonds present.

Table 1. Comparison of bonds in CM and SM

Frequencies (cm^{-1})		Assignments	References
CM	SM		
3277	3408	ν_{as} H–O–H	28
2386	2359	ν_H Si–O–HL O	29
1665	1655	δ_s H–O–H	30
1196, 970	1001	ν_{as} (X)O–Si–O(X) [X = H or Na]	30
893	899	δ_{as} O–Si–O	30
779	760	δ_{as} (H)O–Si–O(H)	30
702	652	δ_{as} (H)O–Si–O(H)	30
461	455	δ_s (H)O–Si–O(Na)	30

1001 cm^{-1} wavenumbers respectively.[29-31] The broad band centred at 3277 cm^{-1} in Figure 1(a) is assigned to the stretching vibration of H_2O in CM. A similar H_2O stretching vibration observed around 3408 cm^{-1} in the spectra of SM (Figure 1(b) may be the result of absorption of atmospheric moisture by the sample.

Compression strength

Compression testing carried out on the sintered sample gave a force-displacement curve shown in Figure 2. There are four distinct stages: in stage I, the material maintains a positive slope until a maximum stress is reached, then ceases temporarily due to the closing up of the micropores, stage II. This is followed by stage III where densification of the pores occurs and the material still shows ability to bear higher loads causing the force-displacement curve to rise again.[32] In stage IV the material collapses completely as more load is applied. This result is in agreement with the general findings on the strength value of porous ceramics.[33] The compression strength of the bioactive glass obtained in this study was 0.37 MPa, while the porosity was 82%. The compression strength of spongy bone, without considering the struts, is in the range of 0.2–4 MPa, when the relative density is ~0.1.[33] Interestingly, our result is within this range although closer to the lower bound and may find useful application in the repair of trabecular bone[6] as well as seeding of cells in bone tissue engineering.

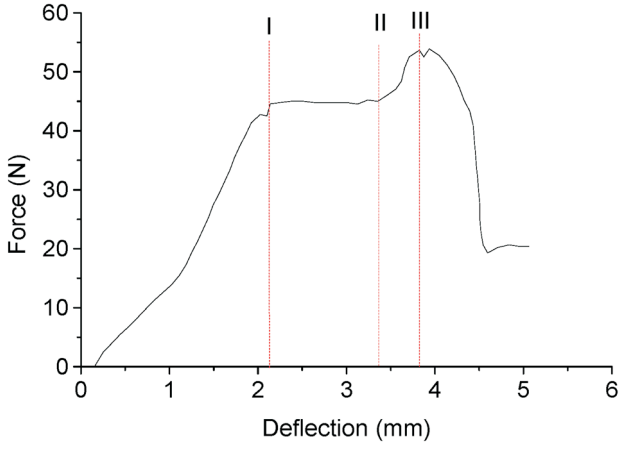

Fig. 2. Force-deflection curve of the bioactive glass sintered at 950 °C for 3 h. The compression strength was 0.37 MPa.

Average pore size of glass

The pore architecture and distribution of the sintered glass material was determined by porometric using SEM (Phenom ProX 800-07334). As shown in the histogram (Figure 3), the pore sizes of the glass are in the range 7-43 μm with the average pore diameter of 13 μm.

Changes in the composition of SBF

Figure 4 shows variation in Na, Si, Ca, and P concentrations in the SBF solution for various periods of immersion of the glass. During the reaction of the glass with the solution, the structure of the glass changes as well as the chemical composition of the SBF due to accumulation of dissolution products from the glass.[18] As it is observed, the concentration of Na in the solution rises rapidly from 142 mM to 343 mM after the first 4 days of soaking and continues to increase slowly to 395 mM after soaking for 14 days. The variation of Si ionic concentration is similar to that of Na. The Si ionic concentration increased rapidly from 0 to 0.91 in 4 days, and reached a constant value of 1.06 mM after 14 days. Ca concentration showed a steep rise for the first 7 days, increasing from 2.5 to 5.38 mM, but slowed

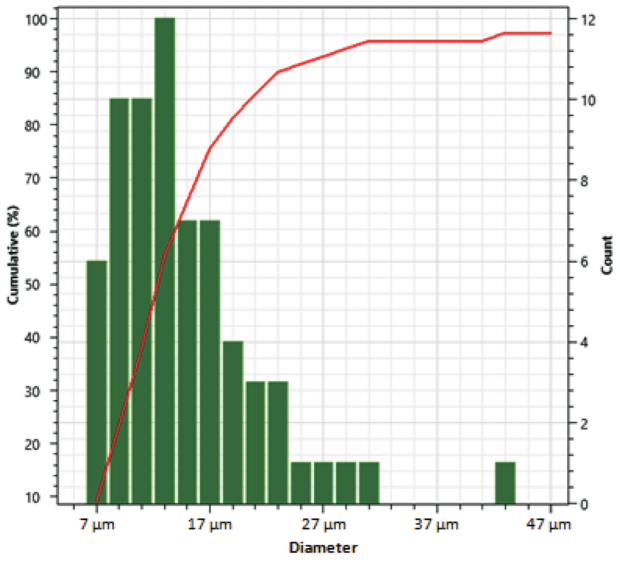

Fig. 3. Histogram showing pore size distribution in the glass.

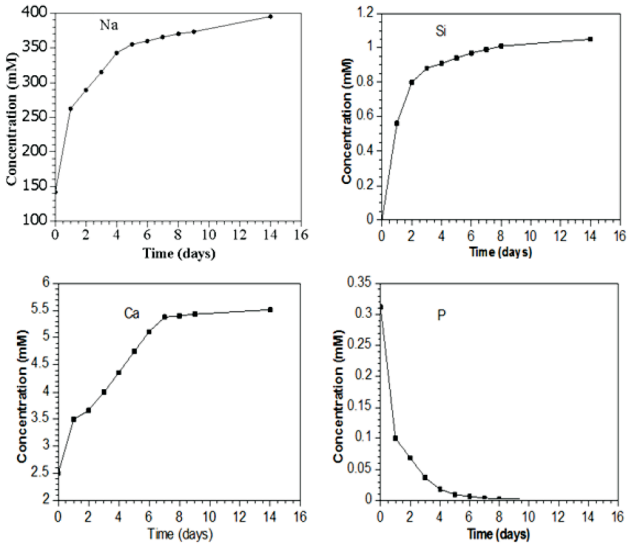

Fig. 4. Variation of Na, Si, Ca and P in the SBF with soaking time.

thereafter stabilizing at 5.44 mM after 14 days. On the contrary, the concentration of P depleted fast from 0.31 mM reaching a constant value of 0.0027 mM after soaking fo 8 days and became exhausted before reaching 14 days.

pH assessment of reactivity and degradability of the glass during immersion in SBF

The variation of pH value relative to soaking times in SBF of the bioactive glass is shown in Figure 5. The increase in pH value from 7.4 to 8.6 during the first four days is due to partial dissolution at the surface of the glass, releasing Na^+ and Ca^{2+} into the solution as shown in the result obtained earlier in Figure 4. This indicates that the glass has high reactivity in biological fluid. This fact agrees with the formation mechanisms of apatite on bioactive glasses and glass ceramics, that is, in the early stages there is fast release of Na^+ and Ca^{2+} ions from the bioactive glass into the surrounding solution followed by an interchange between Ca^{2+} and H_3O^+ from the solution.[34] Such interchanges provoke an increase of the pH that favours the formation of apatite nuclei on the silanol groups on the glass surface.[35] After this stage, there is a slow increase in pH to a saturated value of 8.8 on the 9th day. This can be explained by the release kinetics of Ca^{2+} ions being lower for the glass than its uptake from the SBF solution to form apatite layer on the its surface, and hence corroborates the decline in the rate of increase in concentration of Ca in the solution after 7 days of soaking, which was observed in Figure 4. The pH variation of the bioactive glass supports previous studies on pH changes of gel-derived SiO_2–CaO–Na_2O–P_2O_5 bioactive glasses in biological fluids,[36] thus indicating that the material is reactive and degradable. Critical concentrations of ionic dissolution products from degrading bioactive glasses, such as soluble silica and calcium ions could enhance osteogenesis by regulating osteoblast proliferation, differentiation, and gene expression.[9]

Crystallization and bioactivity of the glass

Changes on the surface of the glass before and after immersion in SBF for different time periods were studied for formation of crystalline phases and transformation of the crystalline phase to HA from the data obtained from SEM, XRD, FTIR and EDX.

SEM

Figure 6 shows the morphology of the glass before and after immersion in SBF. As seen in Figure 6(a), after devitrification, the glass shows a porous network structure of macropores interconnected with micropores, which is in agreement with the porosity value of 82% obtained earlier from calculation using Eq. 2 and the result shown in Figure 3. The glass microstructure appears acicular shaped with associated surface roughness, and as observed, most of the pores are open with struts of average thickness, which may be due to partial crystallization. It is particularly observed that a hollow strut with microstructure walls formed in the glass, as a result of the sintering protocol adopted, which is similar in morphology to sintered bioactive glasses reported in previous works.[32,37] One of the basic requirements of an ideal scaffold is that it should possess an interconnected porous structure, that is, it should be highly per-

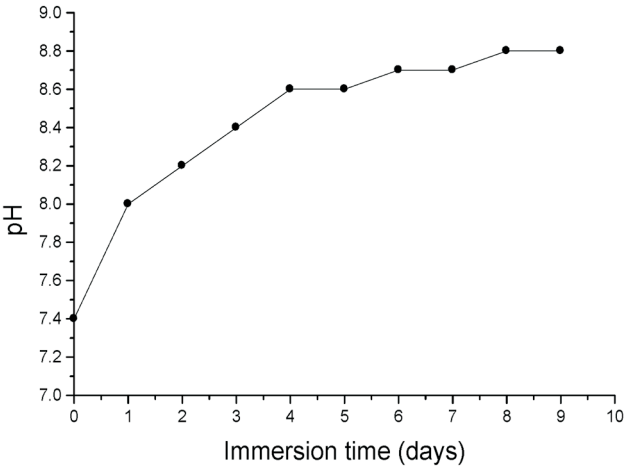

Fig. 5. Changes in pH of the bioactive glass from initial pH = 7.4 during immersion in SBF for the first 9 days.

meable with pore diameter in the range 10-500 μm to allow for for cell seeding, tissue ingrowth and vascularisation as well as nutrient delivery and waste removal.[3,38] Microporosity (≈2–10 μm, < 50 μm) and surface roughness are required for immediate protein and cell adhesion, cell migration and osteointegration.[38,39] The morphology presented by the glass shows properties that match these requirements.

After immersion for 3 days in SBF, apatite began to nucleate on the surface as shown in Figure 6(b) and increased in colony after immersion for 7 days as observed in Figure 6(c). On the 14th day, Figure 6(d), apatite had almost completely populated the surface of the glass, except at the middle region where the glass surface structure is still visible.

XRD

XRD assessment revealed that the sintering protocol led to partial crystallization[32] of the glass as shown in the XRD spectrum, before transferring to SBF for immersion study (at day 0), Figure 7, which confirms the suggestion made earlier during the SEM evaluation. As seen, both angular location and intensity of the peaks match the standard PDF #22.1455, indicating that $Na_2Ca_2Si_3O_9$ was the major phase present.[32] Crystallization temperature of 45S5 Bioglass® is known to be 600 °C.[36] During this heat treatment, $NaNO_3$ and $Ca(NO_3)_2.4H_2O$ decompose to Na_2O and CaO respectively, and combine further with SiO_2 present in the composition to give $Na_2Ca_2Si_3O_9$. Our sintering condition was set at 950 °C for 3 h to balance mechanical competence and biodegradability of the material.[40,41]

There are significant changes in the XRD spectra of the glass after immersion in SBF. Following immersion for 3 days, the intensity of the $Na_2Ca_2Si_3O_9$ peaks decreases and apatite peak is identified at 2θ 32.9. Further immersion led to increase in the number of apatite peaks, whose configurations matched the standard PDF file, JCPDS #9-0432. At day 14, the $Na_2Ca_2Si_3O_9$ peaks had almost disappeared, suggesting that the material is biodegradable and is in conformity with the transformation mechanism of $Na_2Ca_2Si_3O_9$ reported previously.[42,43] Formation of HA, HCA and degradation of the material is an indication that it could be a promising candidate for application in bone repair.

FTIR

Figure 8 shows the FTIR spectra of samples immersed in SBF solution for 0, 3, 7 and 14 days As can be seen, the spectrum of the parent glass before soaking reveals several peaks. The bands at 1119 and 1038 cm^{-1} are associated with Si–O–Si and P–O vibrational modes;[44] 900-964 cm^{-1} are related to Si–O non-bridging oxygen bonds (NBO). The bands around 797 and 475 cm^{-1} are attributed to Si–O–Si bending vibrations. The sharp peaks at 641, 617 and 567 cm^{-1} can be assigned to the presence of

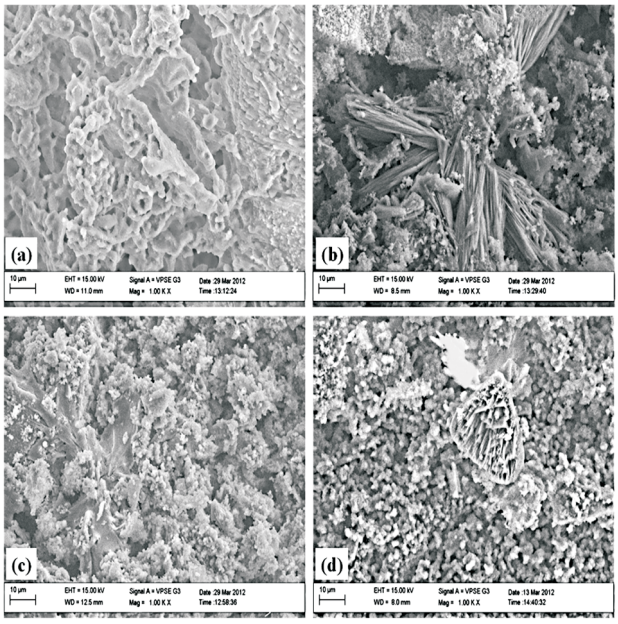

Fig. 6. SEM micrographs of the glass sample sintered at 950 °C for 3 h, (a), and after immersion in SBF for (b) 3 days, (c) 7 days and (c) 14 days. All images at the same magnification.

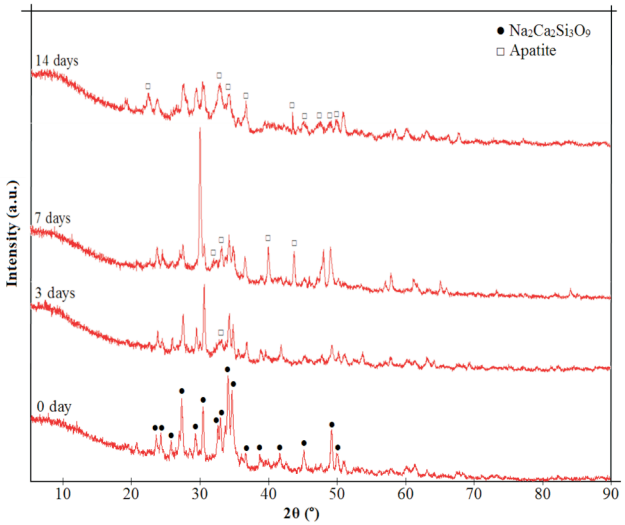

Fig. 7. XRD diffraction patterns of the sintered glass before incubation in SBF (0 day) and after incubation (3 – 14 days) showing growth of HA.

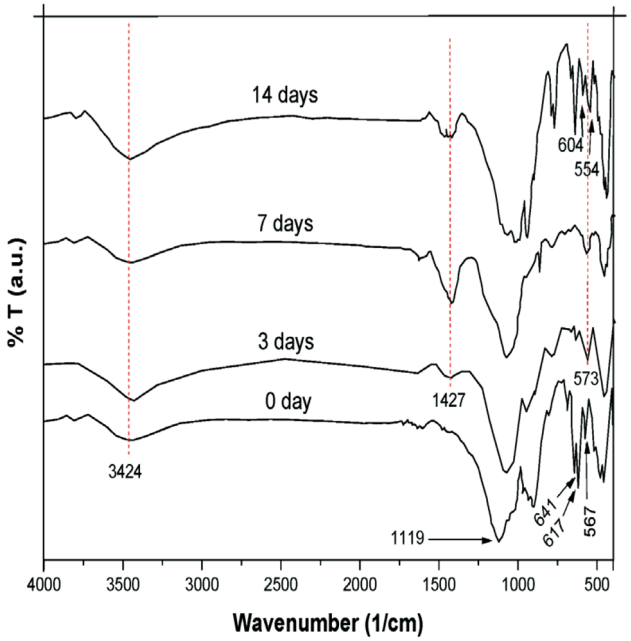

Fig. 8. FTIR Spectra of the glass before immersion (0 day) and after immersion for 3 – 14 days in SBF.

crystalline phase in the sample,[45] which supports the formation of $Na_2Ca_2Si_3O_9$ observed in the XRD result. After soaking for 3 days new peaks emerge at 573 and 1427 cm^{-1}, which are also observable in the spectrum of the sample soaked for 7 days. The peak at 573 cm^{-1} is assigned to P–O bend in amorphous calcium phosphate resulting from formation of HA on the surface of the sample.[46] The band at 1427 cm^{-1}, which became more intense after soaking the sample in SBF for 7 days can be attributed to the presence of CO_3^{2-}, suggesting the onset of CO_3^{2-} into HA. After 14 days of immersion, the bands between 950-1120 cm^{-1} increased in number which may be due to re-polymerization of SiO_2 to form silica rich layer on the glass surface coupled with incorporation of Ca^{2+} re-adsorbed from SBF solution. Additionally, the CO_3^{2-} band becomes broader and develops a second band at 1470 cm^{-1}, while the peak at 573 cm^{-1} splits into two sharp modes at 604 and 554 cm^{-1}, which are characteristic of apatite crystalline phase[46] due to formation of HCA.

EDX

In Figure 9 is shown the EDX spectra of the glass before and after immersion in SBF. The EDX of the parent glass confirms the composition of the glass as prepared. After immersion for 3 days in SBF, the concentration of Na, Ca and Si decreased in accordance with the dissolution theory of bioactive glasses in physiological fluids,[19,47] and consequently P increases slightly due to re-adsorption from the SBF solution, which was observed in Figure 4, to form HA on the surface of the glass. Subsequent immersions led to increase in Ca to form apatite. Additionally, it is observed that at day 14, the intensity of Si was low, correspondingly, that of Ca and P increased, indicating that apatite had colonized the surface of the glass to a large extent. Also, there was an appearance of C in the spectrum of the glass soaked for 14 days, which could be attributed to CO_3^{2-} incorporation to form HCA, thus confirming the FTIR result.

EXPERIMENTAL

Preparation of bioactive glass from sand: The composition of the sand used as source of silica is shown elsewhere.[23] To prepare sodium metasilicate (Na_2SiO_3), the sand ranging in sizes between 159–595 μm was first obtained by passing it through a sieve, then washed thoroughly with deionized water to free it from impurities before drying at 120 °C in an oven for 3 h. Thereafter, 4.00 g of the sand was mixed with 3.53 g of soda ash (Na_2CO_3) and placed in a cavity constructed with bricks. The mixture was fused in a furnace at 1300 °C for 1 h to form Na_2SiO_3 (mole ratio: Na_2O:SiO_2 = 1:2) as shown in Eq. 1.

$$Na_2CO_3 + xSiO_2 \rightarrow (Na_2O).(SiO_2)x + CO_2 \quad (x = 2) \qquad (1)$$

The bioactive glass with composition (mol %) 46.81 SiO_2,

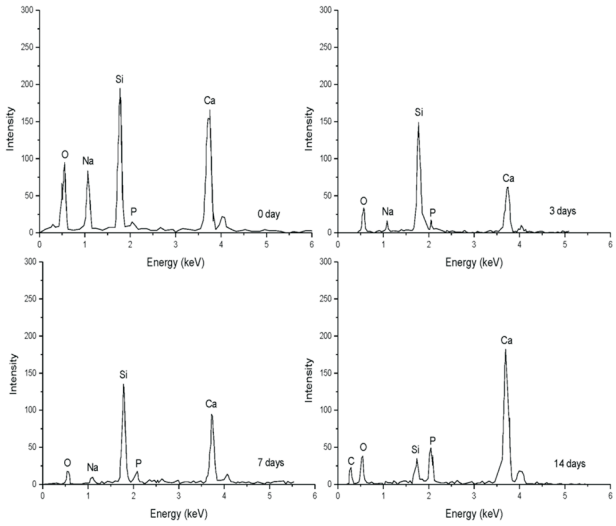

Fig. 9. EDX spectra of the parent glass (0 day) and after soaking in SBF for 3 – 14 days. A distinct peak for carbon (C) can be seen after 14 days in SBF.

24.55 Na_2O, 27.38 CaO and 1.26 P_2O_5, were prepared by mixing the following reagents at room temperature with stirring using a magnetic stirrer in the order: 0.05M HNO_3 (Riedel-DeHaën, 60%) and Na_2SiO_3 liquid (as-prepared from sand), $NaH_2PO_4 \cdot 2H_2O$ (Kermel, 99%) and $Ca(NO_3)_2.4H_2O$ (Loba Chemie, 99%) in the molar ratio of water to the rest of the chemicals of 20:1 to obtain the sol. Each reagent was allowed a maximum reaction time of 45 minutes before adding the next. After adding the final reagent, the mixture was stirred for 1 hour before pouring the resulting sol into teflon moulds and kept at room temperature for 72 h for gelation. The obtained gel was heated at 70 °C for 72 h, 130 °C for 42 h, 700 °C for 2 h and 950 °C for 3 h for aging, drying, stabilization and sintering respectively. The heating and cooling rate was maintained at 5 °C/min.

Characterization: The density ρ_{glass} of the glass was determined from the mass and dimensions of the sintered material. The porosity *P* was calculated by

$$P = (1 - \rho_{glass} / \rho_{solid}) \times 100 \quad (2)$$

where $\rho_{solid} = 2.7$ g/cm^3 is the density of 45S5 Bioglass ®.[35]

The microstructure and composition of the glass was assessed in an EVO/MAIO scanning electron microscope (SEM) equipped with energy dispersive X-ray analyzer (EDX) before and after immersion in simulated body fluid (SBF) for a maximum of 14 days. Silicon substrates were sequentially cleaned with soap and deionized water, ethanol and acetone in an ultrasonic bath and then dried in the oven at 110 °C for 15 min. The samples were thoroughly milled into fine powders and dispersed in an adequate volume of ethanol via ultrasonication for 15 min. The dispersed samples were dropped on the pre-cleaned silicon substrates, placed in an oven at 110 °C for 15 min to dry the ethanol, and then observed at an accelerating voltage of 15 kV.

Samples were characterized using X-ray diffraction (XRD) analysis after sintering and after each immersion experiment in SBF with the aim of assessing the crystallinity and the formation of hydroxyapatite (HA) crystals respectively on samples strut surfaces. The samples were first ground to powder. Then 0.1 g of the powder was measured in a PANalytical Empyrean X-ray diffractometer using CuKα radiation source of wavelength (λ) = 0.154056 nm operated at 40 kV and 40 mA to obtain the diffraction patterns in the 2θ range from 5° - 90°.

Fourier transform infrared (FTIR, Shimadzu 8400S), with wavenumber range of 4000-400 cm^{-1} employing KBr pellets operating in a reflectance mode with a 4 cm^{-1} resolution was used to monitor the nature of bonds present in the samples.

Mechanical Testing: The compression strength of the sintered bioactive glass was measured using a Testometric OL11 INR (Lancashire, England) mechanical tester at crosshead speed of 0.5 mm/min. The samples were cylindrical in shape with dimensions 15 mm in diameter and 30 mm in height. During the compression test, the load was applied until densification of the porous samples started to occur. The compression strength was determined using the relation:

$$\sigma_c = F/\pi r^2 \quad (3)$$

where σ_c is the compression strength, F is the applied load at failure and r is the sample radius.

Assessment of bioactivity in simulated body fluid: Assessment of bioactivity was carried out by the standard *in vitro* procedure[47] using analytical reagent-grade chemicals NaCl, $NaHCO_3$, KCl, $K_2HPO_4 \cdot 3H_2O$, $MgCl_2 \cdot 6H_2O$, $CaCl_2$, trishydroxymethyl aminomethane [Tris-buffer, $(CH_2OH)_3CNH_2$], and 1M HCl with ions concentrations shown in Table 2. Samples were immersed in acellular SBF at concentration of 0.01 g/ml in clean plastic bottles, which had previously been washed using HCl and deionized water. The bottles were placed inside a thermostated incubator at a temperature of 36.5 °C while maintaining pH at 7.4. The SBF solutions were not refreshed throughout the period of immersion. The pH of the solution was checked daily for 9 days using a pH meter (Hanna, HI96107) and ion concentration of the SBF were also monitored daily throughout the period of immersion. Concentrations of Na and Ca were examined by atomic absorption spectrophotometer (AAS) (Perkin Elmer Buck A Analyst); P and Si were estimated by UV/VIS spectrophotometer (Uniscope SM 7504) at wavelengths of 400 and 815 nm respectively. The samples were extracted from the SBF solution after 3, 7 and 14 days respectively. The extracted samples were rinsed with deionized water and left to dry at ambient temperature in a desiccator. The formation of apatite layer on the glass surface was monitored by SEM, EDX, XRD and FTIR.

CONCLUSIONS

A bioactive glass of the SiO_2–Na_2O–CaO–P_2O_5 system using high silica–containing sand as economic starting material was formed by the sol-gel processing method. Af-

Table 2. Ion concentrations (mM) in human plasma in comparison with SBF

Ion	Na^+	K^+	Mg^{2+}	Ca^{2+}	Cl^-	HCO_3^-	HPO_4^{2-}	SO_4^{2-}
SBF	142.0	5.0	1.5	2.5	147.8	4.2	1.0	0.5
Human plasma	142.0	5.0	1.5	2.5	103.0	27.0	1.0	0.5

ter maintaining the sintering condition at 950 °C for 3 h, a crystalline phase, $Na_2Ca_2Si_3O_9$ was produced in the glass. Compression study indicated the glass has strength of 0.37 MPa that falls within the trabecular bone region, attributable to the $Na_2Ca_2Si_3O_9$ phase. Daily evaluation of the composition of the SBF revealed that the glass has a controlled rate of degradation in SBF, a property which could enable it serve as a temporary scaffold pending the formation of a new bone. The significance of this work is that the silica sand route herein compares favourably to previously synthesized sodium–containing bioactive glasses like 45S5 Bioglass® based on TEOS. Interestingly, this route will be highly cost effective as a pathway to candidate bioactive glass scaffolds for application in bone regeneration therapy.

ACKNOWLEDGEMENTS

The authors are thankful to the management of the College of NanoScience and Technology, Soochow University, China for their assistance to run the EDX and XRD of the glass samples in this work.

REFERENCES

1. Stella, J. A.; D'Amore, A.; Wagner, W. R.; Sacks, M. S. *Acta Biomater.* **2010**, *6*, 2365.
2. Perry, C. R. *Clin. Orthop.* **1999**, *360*, 71.
3. Rezwan, K.; Chen, Q. Z; Blaker, J. J.; Boccaccini, A. R. *Biomaterials* **2006**, *27*, 3413.
4. Gerhardt, L.-C.; Boccaccini, A. R. *Materials* **2010**, *3*, 3386.
5. Cao, W.; Hench, L. L. *Ceram*. **1996**, *22*, 493.
6. Jones, J. R.; Lee, P. D.; Hench, L. L. *Phil. Trans. R. Soc. A* **2006**, *364*, 263.
7. Jones, J. R.; Hench, L. L. *Curr. Opin. Solid State Mater. Sci*. **2003**, *7*, 301.
8. Hench, L. L. *J. Am. Ceram. Soc.* **1998**, *7*, 1705.
9. Hench, L. L. *J. Mater. Sci. Mater. Med*. **2006**, *17*, 967.
10. Hench, L. L. *J. Am. Ceram. Soc*. **1991**, *74*, 1487.
11. Fetner, A. E.; Hartigan, M. S.; Low, S. B. *Compend. Cont. Educ. Dent*. **1994**, *15*, 93.
12. Wilson, J.; Douek, E.; Rust, K. In *Bioceramics*; Hench, L. L.; Wilson, J.; Greenspan, D. C., Eds.; *Bioglass Middle Ear Devices: 10 Year Clinical Results*; Pergamon: Oxford, 1995; pp 239-246.
13. Rahaman, M. N.; Day, D. E.; Bal, B. S.; Fu, Q.; Jung, S. B.; Bonewald, L. F.; Tomsia, A. P. *Acta Biomater.* **2011**, *7*, 2355.
14. Brinker, C. J.; Scherer, G. W. *Sol-gel Science–the Physics and Chemistry of Sol-gel Processing*; Academic Press Inc.: New York, 1990; pp 581-582.
15. Hench, L. L.; West, J. K. *Chem. Rev.* **1990**, *90*, 33.
16. Hench, L. L.; Jones, J. R.; Sepulveda, P. In *Future Strategies for Tissue and Organ Replacement*; Polak, J. M.; Hench, L. L.; Kemp, P., Eds.; *Bioactive Materials for Tissue Engineering Scaffolds*; Imperial College Press: London, 2002; pp 3-24.
17. Best, S. M.; Porter, A. E.; Thian, E. S.; Huang, J. *J. Eur. Ceram. Soc.* **2008**, *28*, 1319.
18. Sepulveda, P.; Jones, J. R.; Hench, L. L. *J. Biomed. Mater. Res*. **2002**, *61*, 301.
19. Hench, L. L.; Splinter, R. J.; Allen, W. C.; Greenlee, T. K. *J. Biomed. Mater. Res.* **1971**, *5*, 117.
20. Chen, Q. Z.; Li, Y.; Jin, L. Y.; Quinn, J. M.; Komesaroff, P. A. *Acta Biomater.* **2010**, *6*, 4143.
21. Li, R.; Clark, A.; Hench, L. L. *J. Appl. Biomater.* **1991**, *2*, 231.
22. Jones, J. R.; Sepulveda, P.; Hench, L. L. *J. Biomed. Mater. Res*. **2001**, *58*, 720.
23. Essien, E. R.; Adams, L. A.; Shaibu, R. O.; Olasupo, I. A.; Oki, A. *Open J. Regen. Med*. **2012**, *1*, 33.
24. Nayak, J. P.; Bera, J. *Appl. Surf. Sci*. **2010**, *257*, 458.
25. Crisan, M.; Raileanu, M.; Preda, S.; Zaharescu, M.; Valean, A. M.; Popovici, E. J.; Teodorescu, V. S.; Matejec, V.; Mrazek, J. *Optoelectron. Adv. Mater.* **2006**, *8*, 815.
26. Li, Z.; Hou, B.; Xu, Y.; Wu, D.; Sun, Y.; Hu, W.; Deng, F. *J. Solid State Chem.* **2005**, *178*, 1395.
27. Pabon, E.; Retuert, J.; Quijada, R.; Zarate, A. *Microp. Mater.* **2004**, *67*, 195.
28. McMillan, P. F.; Rammelle, R. L. Jr. *Am. Mineral*. **1986**, *71*, 772.
29. Richard, T.; Mercury, L.; Pouet, F.; d'Hendecourt, L. *J. Colloid Interface Sci*. **2006**, *304*, 125.
30. Bernal, S. A.; Provis, J. L.; Rose, V.; de Gutierrez, R. M. *Cement Concrete Comp*. **2011**, *33*, 46.
31. Halasz, I.; Agarwal, M.; Li, R.; Miller, N. *Micropor. Mesopor. Mater.* **2010**, *135*, 4.
32. Chen, Q. Z.; Thompson, I. D.; Boccaccini, A. R. *Biomaterials* **2006**, *27*, 2414.
33. Peitl, O.; LaTorre, G. P.; Hench, L. L. *J. Biomed. Mater. Res*. **1996**, *30,* 509.
34. Zhong, J. P.; LaTorre, G. P.; Hench, L. L. In *Bioceramics;* Andersson, O. H.; Yli-Urpo, A., Eds.; *The Kinetics of Bioactive Ceramics Part VII: Binding of Collagen to Hydroxyapatite and Bioactive Glass*; Butterworth-Heinemann: London, 1994; pp 61-66.
35. Hench, L. L.; Wilson, J. *Science* **1984**, *226*, 630.
36. Siqueira, R. L.; Peitl, O.; Zanotto, E. D. *Mater. Sci. Eng. C* **2011**, *31*, 983.
37. Montanaro, L.; Jorand, Y.; Fantozzi, G.; Negro, A. J. *Eur. Ceram. Soc*. **1998**, *18*, 1339.
38. Karageorgiou, V.; Kaplan, D. *Biomaterials* **2005**, *26*, 5474.
39. Woodard, J. R.; Hilldore, A. J.; Lan, S. K.; Park, C. J.; Morgan, A. W.; Eurell, J. A.; Clark, S. G.; Wheeler, M. B.; Jamison, R. D.; Wagoner Johnson, A. J. *Biomaterials* **2007**, *28*, 45.
40. Clupper, D. C.; Mecholsky, J. J. Jr.; LaTorre, G. P.;

Greenspan, D. C. *Biomaterials* **2002**, *23*, 2599.
41. Clupper, D. C.; Hench, L. L. *J. Non-Cryst. Solids* **2003**, *318*, 43.
42. Carta, D.; Pickup, D. M.; Knowles, J. C.; Smith, M. E.; Newport, R. J. *J. Mater. Chem*. **2005**, *15*, 2134.
43. Peitl, O.; Zanotto, E. D.; Hench, L. L. *J. Non-Cryst. Solids* **2001**, *292*, 115.
44. Lefebvre, L.; Chevalier, J.; Gremillard, L.; Zenati, R; Thollet, G.; Bernache-Assolant, D.; Govin, A. *Acta Mater.* **2007**, *55*, 3305.
45. Mami, M.; Lucas-Girot, A.; Oudadesse, H.; Dorbez-Sridi, R.; Mezahi, F.; Dietrich, E. *Appl. Surf. Sci.* **2008**, *254*, 7386.
46. Oliveira, J. M.; Correia, R. N.; Fernandes, M. H. *Biomaterials* **2002**, *23*, 371.
47. Kokubo, T.; Takadama, H. *Biomaterials* **2006**, *27*, 2907.

